Tellus (1995), 47B, 103–121
Printed in Belgium – all rights reserved

TELLUS
ISSN 0280–6509

Modelling the seasonal course of the upper ocean pCO_2 (I). Development of a one-dimensional model

By DAVID ANTOINE* and ANDRÉ MOREL, *Laboratoire de Physique et Chimie Marines, Univ. P. & M. Curie, CNRS (URA 353), 06230 Villefranche sur Mer, France*

(Manuscript received 12 November 1993; in final form 1 August 1994)

ABSTRACT

A one-dimensional model is developed to simulate the seasonal course of the mixed-layer CO_2 partial pressure (pCO_2) at a given oceanic site. This rather detailed numerical tool is particularly designed to quantify the relative role of physical and biological processes in the modulation of the pCO_2. It accounts for (i) the variations in the physical environment, i.e., mixed-layer depth, temperature and eddy diffusivity, in response to the external forcing, (ii) the photosynthetic carbon fixation, (iii) the fate of the organic carbon produced through photosynthesis, either locally recycled or exported down to deep waters, and which is parameterised by using the temporal variations of the chlorophyll content combined with a *f*-ratio, (iv) the chemistry of CO_2 in seawater, allowing the pCO_2 inside the mixed layer to be computed from the total inorganic carbon (ΣCO_2) and total alkalinity (TA) contents. The carbon fluxes resulting from air-sea exchange, upward transport, and net primary production are thus simultaneously assessed. The model is purposely developed under the constraint of using (almost exclusively) remotely-sensed data, namely those about chlorophyll, wind, temperature, and incident irradiance; nevertheless, an a priori knowledge of the oceanic zone under consideration and corresponding variables is required when initializing the model. If the photosynthetic carbon uptake is explicitely accounted for, the model, however, cannot predict the algal biomass evolution. On the contrary, it is driven by this evolution and the chlorophyll concentration, as detectable from space, is the main input into the carbon-based biological compartment of the code.

1. Introduction

The development of physical and numerical tools which are able to use contemporaneous satellite information about, e.g., ocean colour, temperature, wind speed and cloudiness, in view of inferring carbon fluxes, is a major challenge for present oceanography. The ultimate goal is the global estimate of the air-sea CO_2 net flux, given that the exchange (in both directions) is sized by the partial pressure difference between atmosphere and ocean (ΔpCO_2), combined with the wind-dependent gas-exchange coefficient at the interface. The parallel goal is to predict the carbon fluxes towards the interior of the ocean.

Between space observations and the desired in-water parameters, there is a serious gap; various problems are to be faced when attempting to understand and predict the oceanic CO_2 partial pressure (pCO_2) from the restricted number of variables observable from space. To the extent that the atmospheric CO_2 partial pressure, compared to that of oceanic upper layers, is more stable with respect to time and space as well as more easily documented, the major problem lies in the highly variable character of the oceanic pCO_2 field and in its mesoscale or even small-scale structure (Gordon et al., 1973; Goyet et al., 1991; Kempe and Pegler, 1991; Metzl et al., 1991; Watson et al., 1991).

This variability results from intermingled processes occuring within the upper ocean. In a

* Corresponding author.

simplified envision, they can be summarised as both the "solubility pump" for atmospheric CO_2, depending on the sea-surface temperature (SST) and the diffusivity within the water body, and the "biological pump", which depends on primary production and local consumption. The yield of the first pump is enhanced as SST decreases (Weiss et al., 1982), while an increase of the downward flux of biologically-produced organic carbon intensifies the efficiency of the second pump. Both pumps are also influenced by vertical motions in different manners. Downward entrainment and deep convection not only bring newly dissolved atmospheric CO_2 into deeper levels, but also perturb the vertical distribution of algae and their photosynthetic activity. In contrast, upward motions of CO_2-supersaturated and also nutrient-rich deep waters lead to ΣCO_2 increase and also enhanced incorporation of inorganic carbon into biota. This general functioning determines the broad outline of the localisation within the world ocean of sink or source zones for atmospheric CO_2, and lays the basis for global "box-models" approaches (Volk and Liu, 1988; Volk and Bacastow, 1989). However large uncertainties remain about the reservoirs and fluxes considered in, or derived from, such studies (Longhurst, 1991). Furthermore, the picture is also getting complicated when these processes are examined at smaller time and space scales.

Thus, before attempting to estimate at large scale sea-surface pCO_2 fields from satellite data, a one-dimensional modelling is a preliminary and appropriate way to quantitatively understand the respective influences of the various processes involved in the pCO_2 evolution. Numerous studies were recently carried out along this line. For example, Peng et al. (1987), developed a 2-box model, based on a simple parameterisation of physical and biological processes, attempting to reproduce measured pCO_2. Taylor et al. (1991), examined the response of ΣCO_2, the total inorganic content, and of pCO_2 to a phytoplankton bloom in "academic situations" differing by their latitudes; physics of the mixed layer, however, was imposed in their modelling investigation. By using an upper-ocean model for mixed-layer prediction, Garçon et al. (1992) carried out a detailed study of the variability of pCO_2 within the upper ocean, combined with a prescribed primary production cycle.

From these studies, from field observations (Wong and Chan, 1991; Wong et al., 1993; Schneider et al., 1992), and also from recent synthesis about the carbon cycle (e.g., Longhurst, 1991), it is obvious that weaknesses subsist in the suite of parameterisations needed to retrieve the pCO_2 variations, in particular in the way of reproducing the impact of the biological activity. It is now feasible to estimate the total primary production from chlorophyll, incident solar radiation and appropriate physiological parameters, by using space-acquired ocean colour data, from which the pigment concentration can be derived (Platt and Sathyendranath, 1988; Morel and André, 1991). A relevant piece of information is still missing in the CO_2 problem, as long as the local recycling (remineralisation) rate of the organic carbon produced by autotrophs remains to be quantified. For a given total primary production, an extremely high recycling rate (all the organic carbon being locally consumed and released as CO_2) would imply no effect of biological activity on pCO_2. In the converse case (no recycling), the CO_2 drawdown within the upper ocean would be equal to the total primary production. Most of the situations are between these two extreme figures. The chemical and ecological backgrounds, which govern the intensity of the biologically-induced variations in ΣCO_2, and also determine the depth where they occur, are quite complex. The processes involved include, not exhaustively, photosynthetic organic carbon formation, CO_2 release through oxidation and respiration by autotrophs and heterotrophs, vertical migration of zooplankton and occasionally calcium carbonate formation.

With the purpose of simulating in a realistic way annual cycles of the mixed-layer pCO_2, a one-dimensional model of the upper ocean has been developed. It includes the physics of the mixed layer, the biochemical effects of primary production and carbon recycling. The model is not entirely free nor self-sufficient. It makes continuous use of several sources of data, preferably detectable from space (SST, solar irradiation, wind, algal pigments) and requires, when initialising the computation, an a priori knowledge of the oceanic zone under consideration (salinity, ΣCO_2 and temperature profiles). The adoption of, at least, a mean "f value", i.e., a value of the ratio of new-to-total production (Dugdale and Goering,

1967), is also necessary. An overview of the model, and then a detailed description of its segments, are provided.

2. General features of the model

The model is built to account for the following processes: heat, momentum and CO_2 transfer at the ocean-atmosphere interface, eddy diffusivity, variations in temperature, salinity and depth of the mixed layer, and finally the biological activity, including its two aspects, the photosynthetic carbon fixation by autotrophs and the regeneration by consumers. All these processes affect the ΣCO_2 and the total alkalinity (TA) of the water body, and accordingly modify the pCO_2 level inside the upper oceanic layer (see Table 1 for symbols thereafter used in the text).

The model considers a one-dimensional system, with a water column extending from the ocean-atmosphere interface to a prescribed depth (hereafter 300 m), and with a deep reservoir where all chemical species are assumed to be constant over time. The upper boundary is the ocean-atmosphere interface, where CO_2, heat and momentum exchanges take place; the lower boundary is the interface with the deep reservoir, through which the water-column can exchange chemical compounds. Inside the water column, there are two particular horizons, the mixed-layer depth, noted Z_{ml}, and the bottom of the "productive layer", noted Z_p. Depending on the stability of the water body and the algal content, these two layers generally differ in thickness and two situations may happen ($Z_{ml} > Z_p$ or $Z_{ml} < Z_p$, see Fig. 1). Z_p is assumed to be 1.5 times the euphotic depth as usually defined, namely that depth where the downwelling PAR-irradiance is reduced to one per cent of its surface value (PAR, the photosynthetically available radiation, is the radiant solar energy within the 400–700 nm spectral range). The factor 1.5 accounts for any possible carbon fixation below the somewhat arbitrary "one per cent level".

The physical characteristics of the mixed layer are derived from an eddy kinetic energy model (Gaspar et al., 1990), driven by surface heat fluxes and wind stress. The mixed layer is assumed to form a rigorously homogeneous medium, in such a way that all the concentrations are uniformly dis-

Table 1. *Symbols and units used in the text (except those used in Appendices)*

pCO_2	Oceanic CO_2 partial pressure (μatm)
ΣCO_2	Total inorganic carbon concentration in seawater (μ mol kg^{-1})
ΔpCO_2	CO_2 partial pressure difference at the air-sea interface (μatm)
TA	Total alkalinity in the mixed layer (μequ kg^{-1})
NO_3	Nitrate concentration (mol m^{-3})
O_2	Oxygen concentration (mol m^{-3})
Chl	Chlorophyll concentration (mg Chl m^{-3})
PAR	Photosynthetically available radiation: radiant solar energy within the 400–700 nm spectral range (μE m^{-2} s^{-1})
Z_p	Depth of the productive layer (m). Z_p is 1.5 times the euphotic depth, that is that depth where PAR is reduced to 1 % of its value just below the sea surface.
Z_{ml}	Depth of the mixed layer (m)
EKE	Eddy kinetic energy (m^2 s^{-2})
K_z	Eddy diffusivity coefficient (m^2 s^{-1}, and subscript ml for its value at the base of the mixed layer)
SST	Sea-surface temperature (°C)
k	gas transfer velocity (m s^{-1})
α	solubility of CO_2 in sea water (mol CO_2 m^{-3} μatm^{-1})
P	Net primary production (gC m^{-2} d^{-1}, and subscript d for a daily rate).
L	Carbon loss from the productive layer (gC m^{-2} d^{-1}, and subscript d for a daily rate)
R	Local recycling of the organic carbon produced through photosynthesis (gC m^{-2} d^{-1}, and subscript d for a daily rate)
X	Export out of the productive layer of the organic carbon produced through photosynthesis (gC m^{-2} d^{-1}, and subscript d for a daily rate)
C-to-Chl	Carbon-to-Chlorophyll ratio (g/g)
f	Ratio of new-to-total production

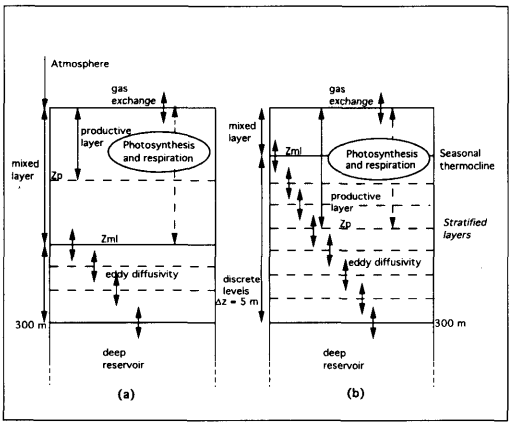

Fig. 1. Diagram showing the processes accounted for by the present model, and their respective vertical positions, (a) when the mixed layer is deeper than the productive layer and, (b) for the converse situation. CO_2 and O_2 gas-exchanges occur through the air-sea interface; photosynthesis and respiration (re-mineralisation) take place within the productive layer; eddy diffusivity carries CO_2, O_2 or NO_3 between the deep layers and the mixed layer, in a direction depending on the sign of the vertical gradient. It is worth noting that in (a), photosynthesis and respiration only take place within the productive layer. The biologically-induced variation in ΣCO_2 extends however to the whole mixed layer.

tributed with respect to depth; as a consequence, the quantities exchanged through its lower and upper boundaries are supposed to be instantaneously shared by all parts of the mixed layer.

The carbon-based biological compartment of the modelling is ruled both by the chlorophyll (Chl) concentration and the amount and spectral distribution of PAR at the sea surface (Morel, 1991). It provides the net carbon fixation rates by autotrophs at all levels. From these primary production estimates, combined with the time-variations of the Chl content, the proportions of local recycling of organic carbon within the productive layer and of export to deeper levels are evaluated. Along with the ΣCO_2 changes, the oxygen evolution is stoechiometrically derived from the estimates of the new and recycled production. Nitrate variations can also be derived by using the C-to-N Redfield ratio. These concentrations, however, are never used to constrain the modelling of the biological activity; they conversely are outputs of the simulation, yet useful for the global validation.

The values of all the compartments of the biogeochemical model (ΣCO_2, TA, O_2 and NO_3 vertical profiles) are initialized each day with their value obtained at the end of the previous day (or with initializing values for the first day of simulation). At each time step (1 day), the biologically-induced ΣCO_2 variations are evaluated within the entire homogeneous mixed-layer, and within each of the stratified deep layers with a vertical resolution of 5 meters. These CO_2 source/sink terms, the initial ΣCO_2, TA, O_2 and NO_3 values, and the physical forcing for the day in question are then introduced within an iterative scheme (see Appendix F). When convergence is reached, carbonate chemistry with the relevant equilibrium constants is introduced to compute, from ΣCO_2 and TA within the mixed layer, the pCO_2 within this layer. Both the ΔpCO_2 and the CO_2 air-sea exchange are thus straightforwardly obtained. The possible change in TA due to the nitrate uptake (Goldman and Brewer, 1980) is taken into account, as well as the changes in ΣCO_2 and TA due to the formation of calcium carbonate. Total alkalinity can also be modulated by salinity variations, if any. The carbon, oxygen and nitrate fluxes resulting from eddy diffusivity, air-sea exchange and export of organic carbon are also computed.

It is worth emphasizing that the present modelling is purposedly controlled by surface parameters only. Information regarding to the in-water structure are exclusively needed for the initialisation phase. This voluntary restriction conforms to the aim of developing a tool adapted to the data as delivered by satellite sensors. Along the same line, and according to the essence of the primary production model, where photosynthesis is not nutrient-controlled, the chlorophyll biomass is not a product of the simulation. It is conversely an input in the computational scheme and the corresponding data source is expected to be an ocean colour operating system.

3. Detailed description of the model segments

The entire modelling is schematically shown in Fig. 2, and the required inputs are summarised in Table 2. The detailed equations relevant to each of the following segments of the model are provided in Appendix F.

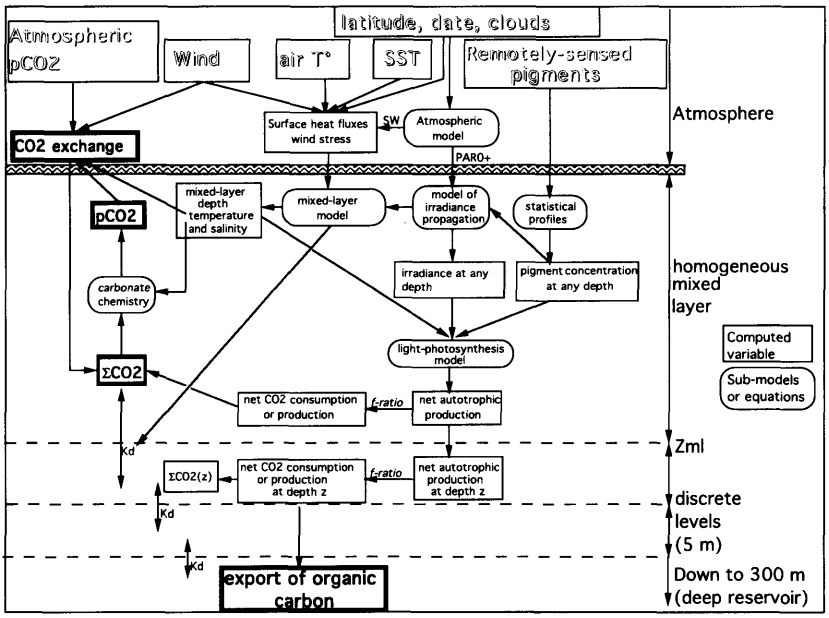

Fig. 2. Diagram showing all the interactions and dependencies accounted for by the present model. Double-headed arrows show a CO_2 exchange, either at the air-sea interface, or between successive levels, whereas simple arrows either symbolise the influence of one parameter on an other one, or represent an input to a sub-model. Nitrate and oxygen are not shown for the sake of clarity; they are actually derived quantities and are not involved in the computations.

3.1. Upper-ocean mixed layer characteristics and eddy diffusivity

The eddy kinetic energy (EKE) model of Gaspar et al. (1990) is designed to simulate vertical mixing at all depths within a water column. The equations for conservation of heat, salt, and momentum are solved and turbulent fluxes are parameterised using the concept of eddy diffusivity (see Appendix A). For detailed information about these equations and the kinetic energy closure scheme, reader is referred to Gaspar et al. (1990), and also to recent studies based on this model (Garçon et al., 1992; Thomas et al., 1993). The EKE is driven by (i) the solar flux incident at the sea surface, and then by its progressive absorption through the water column, (ii) the "non solar flux", i.e., the sum of the latent and sensible heat fluxes and of the net long-wave radiation budget, (iii) the surface water balance and (iv) the wind-stress at the sea surface. The way of estimating these fluxes is explained in Appendix A. With respect to previous uses of this EKE model, three significant modifications have been introduced (their usefulness is discussed in the frame of a validation of the model).

(i) In place of using the parameterisation of Paulson and Simpson (1977), constant throughout the year and tuned according to a selected Jerlov's (1976) optical water type, the propagation of solar radiations is made dependent upon the actual chlorophyllous pigment concentration, and is accordingly parameterised (Morel and Antoine, 1994).

(ii) The estimation of the mixed-layer depth is also modified. Gaspar et al. (1990) considered that, starting from the surface, the first value of the turbulent kinetic energy that is lower than a selected threshold (i.e., $10^{-6}\ m^2\ s^{-2}$) is the footprint of the mixed layer bottom. When adopting this criterion, the impact of very rapid retreat events appears to be exagerated; they may last two or three days, when a first relative (and often weak) minimum of kinetic energy momentarily develops at a relatively shallow depth. This criterion was modified as follows; instead of the first relative minimum, the deepest value still

Table 2. *Parameters needed to drive the model and the possible source(s) from which they could be obtained for future studies, making use of satellite observations*

Parameter	Symbol	Parameter or processes relying upon	Possible source
sea-surface temperature	SST	(i) physics of the mixed layer (ii) gas exchange (iii) carbonate chemistry (iv) primary production	remotely-sensed temperatures
salinity	S	(i) physics of the mixed layer (ii) gas exchange (iii) carbonate chemistry	climatological profiles
air temperature	T_a	(i) physics of the mixed layer	meteorological/weather forecast centers
wind speed	V_{10}	(i) physics of the mixed layer (ii) CO_2 gas exchange	remotely-sensed wind speeds from scatterometers, or from meteorological/weather forecast centers
clear-sky irradiance at the surface and clouds	SW PAR	(i) physics of the mixed layer (ii) primary production	remotely-sensed data, or models, or meteorological/weather forecast centers
CO_2 partial pressure in air	PCO_2	(i) CO_2 gas exchange	atmospheric PCO_2 monitoring
near-surface chlorophyllous pigments	Chl	(i) primary production (ii) solar heating rate	ocean color remote-sensing
physiological parameters		(i) photosynthesis primary production	plant physiology
f-ratio C-to-Chl ratio		(i) organic carbon recycling and carbon export	oceanographic surveys

greater than the threshold is adopted as being the actual depth of the mixed layer.

(iii) In the routine version of the model, three-hourly estimates of the heat fluxes are introduced into the EKE. The outputs are the three-hourly values of the mixed-layer depth, of the temperatures and of the eddy diffusivities from the surface down to 300 m, with a five meter depth increment (the model could also accomodate different time scales). The last modification consists of considering this mixed layer as strictly homogeneous, forming a unique box for the biological and chemical processes. The constant temperature for this homogeneous mixed layer is simply computed by averaging the temperatures obtained by the EKE model from 0 down to Z_{ml}; actually the temperature fluctuations around the mean, within the mixed layer, are usually no greater than $\pm 0.1°C$, and exceptionally $\pm 0.5°C$ in summer. The eddy diffusivity vertical structure throughout the mixed layer is ignored. Temporal averaging is also made, to produce daily values, in concordance with the time step adopted for the biogeochemical model. The mixed-layer temperature and the eddy diffusivity vertical profiles (beyond Z_{ml}) are thus assumed to be constant during a day and changing from day to day in the following segments of the model. Nycthemeral variations are therefore ignored.

Exchanges of ΣCO_2, NO_3 and O_2 between the mixed layer and the underlaying levels are determined by the daily value of the eddy diffusivity at the base of the mixed layer. During entrainment periods, the layers newly "incorporated" within the mixed layer contribute to modify its mean concentration according to a mixing rule. Under the mixed layer, eddy diffusivity is the sole physical process responsible for changes in the ΣCO_2, O_2

and NO_3 concentrations. The deep (constant) reservoir is not affected by the exchanges with the water column. Chemical compounds are however permanently dipped into the deep reservoir, which acts as a restoring box (see Appendix F for detailed equations).

3.2. *CO_2 and O_2 gas-exchange through the atmosphere-ocean interface*

The CO_2 flux at the ocean-atmosphere interface, F, is determined by the ΔpCO_2 (μatm) and by the CO_2 gas-exchange coefficient (mol CO_2 m^{-2} s^{-1} μatm^{-1}), which is the product of k, the gas transfer velocity (m s^{-1}), and of α, the CO_2 solubility in seawater (mol CO_2 m^{-3} μatm^{-1}).

$$F = k\alpha\, \Delta pCO_2.$$

Following Liss and Merlivat (1986), k is computed from wind speed and a temperature-dependent Schmidt number, and α from temperature and salinity according to Weiss (1974). The computed daily value of F is simply added to, or subtracted from, the mixed-layer total CO_2 concentration. The formulation is essentially the same for O_2, using a temperature and salinity dependent solubility (Weiss, 1970), and the relevant Schmidt number for O_2.

Note that the gas-exchange mechanisms take place within the sea-surface microlayer, and that the bulk value of the partial pressure is not strictly the relevant quantity to be considered when wind speed is low, typically under 10 m s^{-1} (Robertson and Watson, 1992). Two other phenomena not considered are (i) the possible barrier to gas-exchange created by a stagnant film of dissolved organic matter and (ii) the trapping of air bubbles (Wanninkhof, 1992; Thomas et al., 1990). The extent to which neglecting these processes can bias the flux estimates is not examined.

3.3. *Algal biomass*

As usual, the Chl concentration is used as a descriptor of the algal content. In the perspective of relying on remotely sensed data, the supposedly known Chl concentration to be used as input in the model is $Chl_{\langle sat \rangle}$, i.e., this concentration within the upper layer which can be detected by a satellite-borne ocean colour sensor (Gordon and McCluney, 1975). The carbon fixation of algae, however, occurs in a much (4–6 times) thicker layer and its prediction requires a knowledge of the entire biomass profile. With this aim, a statistical analysis of about 4000 vertical Chl profiles from the world ocean was carried out (Morel and Berthon, 1989), leading to empirical formulations, here adopted. In summary, the column-integrated Chl content has been statistically related to $Chl_{\langle sat \rangle}$ and two situations have been separately considered: when deep convection processes occur (winter, moderate and high latitudes) or when waters are stratified (low, and moderate latitudes in summer). In the first case, there is no vertical structure and the column content is obtained by integrating over the appropriate depth the uniform Chl profile. In the second case, the relationship between $Chl_{\langle sat \rangle}$ and the integrated amount is different (see Appendix B) and the structure of the vertical profile can be statistically related to the surface value. Based on these statistical relationships, a prognostic equation has been proposed and the vertical Chl distribution is modelled as a varying Gaussian profile (Lewis et al., 1983) superimposed on a background concentration and the depth, width and magnitude of the Gaussian peak have been operationally related to $Chl_{\langle sat \rangle}$. According to this model, the Chl distribution in stratified waters evolves from a profile with a sharp, intense and deep Chl maximum in oligotrophic waters (low $Chl_{\langle sat \rangle}$) to a smoother profile with a broad maximum at the surface in eutrophic waters (high $Chl_{\langle sat \rangle}$).

In conformity with the present model hypothesis of a perfectly homogeneous mixed layer, the Chl concentration within this layer is given a strictly constant value, equal to the mean value derived from the profile over the same depth interval. Below the mixed layer, where stable stratification takes place, the reconstructed profile is kept unchanged. With this Chl profile, the PAR energy is propagated downward according to Morel (1988) (as summarized in Appendix C).

3.4. *Net primary production (P)*

The amount of carbon fixed by algae is computed from the chlorophyll distribution and from the PAR vertical profile including its changing spectral composition, by using a spectral light-photosynthesis model previously developed (Morel, 1991). The computation rests on the growth rate equation of Kiefer and Mitchell (1983). This equation expresses that the local and instantaneous

carbon fixation, dC/dt, results firstly from absorption of photosynthetically available radiation (at given depth, instant and wavelength, z, t, and λ) by algae having a Chl-specific absorption coefficient $a^*(\lambda)$, and then from transformation of the absorbed energy (quanta) into chemical energy (stored into the photosynthetized organic matter) via a quantum yield φ, so that:

$$dC(z, t, \lambda)/dt = 12\ \mathrm{PAR}(z, t, \lambda)\ a^*(\lambda) \times \mathrm{Chl}(z)\ \varphi(z, t, \lambda),$$

where 12 is the molar weight of Carbon. This equation is then triply integrated with respect to λ, t, and z, over the photosynthetically active spectrum (400–700 nm), the daylength and the depth of the productive layer (depending on the Chl profile, which also governs the light penetration). The practical ways of modelling the quantum yield and performing the integrations are summarized in Appendix D.

The computed primary production, thereafter denoted P, is postulated as being a "net" production, because, when modelling the quantum yield, a maximum quantum yield for growth is selected (instead of a higher maximum quantum yield for photosynthesis), so that the Carbon loss due to respiration by autotrophs is implicitely accounted for. In such a scheme, parameterising a nutrient limitation for phytoplankton growth is not appropriate, since primary production is computed on a day-to-day basis and derived from the (daily) actual Chl content. This content as well as its vertical distribution already reflects the trophic status of the algal population and the influence of previous nutrient availability that has fixed the standing stock at its present level. The areal net production ($\mathrm{gC\ m^{-2}\ d^{-1}}$) within the mixed layer or within the entire productive layer are separately obtained by integrating the local production ($\mathrm{gC\ m^{-3}\ d^{-1}}$) from the surface down to Z_{ml} or Z_{p}, respectively.

3.5. *Carbon recycling within the productive layer, and export of organic carbon to deeper levels*

To assess the global effect of biological activity on the ΣCO_2, it is necessary to estimate this part, R, of the net primary production (P) which is locally consumed, leading to a CO_2 release. The remaining part, $P - R$, is partitioned between the net increase of the organic carbon pool and the net export of organic carbon towards deeper levels.

It is generally stated (Platt et al., 1989) that the exportable carbon is equal to the "new", essentially nitrate-based, production (Dugdale and Goering, 1967). This equality can only hold true under the hypothesis of long-term equilibrium, namely of a steady state of the carbon biomass (for instance, from year to year). In such an envision, R should be equated to the regenerated production

$$R = P(1 - f),$$

where f is the ratio of new-to-total production (Dugdale and Goering, 1967; Eppley and Peterson, 1979). On a daily basis, however, the new production, which relies on the nature of the nitrogen supply, and the carbon export, which relies on the contemporaneous structure of the foodweb, are not necessarily closely related (e.g., discussion in Legendre and Gosselin, 1989; Quiñones and Platt, 1991; Laws, 1991). In addition, over a short period of time, the algal biomass is generally evolving, either declining or increasing. Another complexity originates from the definition of f. This parameter is defined for the entire productive layer, regardless of the different regimes prevailing inside and below the mixed layer, while these two regimes must be separately considered in the present computation.

To the extent that the assumption of steady state is not compatible with the temporal resolution adopted for the model (1 day), the above equation cannot straightforwardly apply. At this time scale, the algal biomass evolution cannot be ignored. Meanwhile the bulk f value, assumed to be typical of the season and region considered, has to be respected, even if the daily values of this parameter, denoted f_{d}, are possibly changing. This double constraint is the rationale for deriving a time-dependent estimate of R, based on the knowledge of the Chl evolution (as detectable from space, for instance).

In principle, the derivative with respect to time of the column integrated Chl content allows an organic carbon "loss" to be assessed. The reasoning, which implies the adoption of a carbon-to-chlorophyll ratio (C-to-Chl), is as follows: given a Chl biomass at a given date, the primary production model predicts the daily incorporation of carbon. This amount is transformed into a theoretical increase of Chl, $\Delta(\mathrm{Chl})_{\mathrm{t}}$, which can be

compared to the actual increase after one day, $\Delta(\mathrm{Chl})_a$. The difference appearing between these two quantities, δ Chl ($=\Delta(\mathrm{Chl})_t - \Delta(\mathrm{Chl})_a$), once re-transformed into carbon, represents the daily carbon loss from the productive layer, denoted L_d. This loss results from two distinct processes, namely the local consumption of organic carbon, R_d, (converted back to CO_2) and the organic carbon export (sinking), X_d; R_d implicitely includes processes like grazing and remineralisation; X_d is assumed to exit the model domain, its remineralisation occuring below the maximum depth considered. Therefore, the quantity L_d must be partitioned according to

$$L_d = R_d + X_d$$

with $R_d = L_d(1 - f_d)$, and $X_d = L_d f_d$, and where the subscript d means daily rates. Several situations can occur, as follows:

$L_d < 0$, the primary production model is wrong (it underestimates the production), or the C-to-Chl ratio is misadapted. A provision for such a situation is made in the code (L_d is reset to 0).

$L_d = 0$, all the carbon fixed by photosynthesis remains incorporated into the biomass; in such a case, the effect of biological processes on ΣCO_2 is strictly equal to $-P_d$.

$P_d > L_d > 0$, the biomass is still increasing despite the existence of a loss; a certain part of the CO_2 fixed is regenerated and the depressive effect on ΣCO_2 is less than in the previous situation, being now $-P_d + L_d(1 - f_d)$.

$L_d = P_d$, the biomass is stable; if hypothetically f_d was set to zero (entirely regenerated production), then ΣCO_2 would be unaffected, leading to a situation equivalent to that of an abiotic ocean. If more realistically f_d differs from zero, the new production is entirely exported.

$L_d > P_d$, the biomass is declining; such a system can either depress or enhance ΣCO_2, depending on the value of f_d, and of the ratio L_d/P.

It must be pointed out that, with this approach, the daily rates, R_d and X_d, are allowed to be fluctuating, under the proviso that after summing over a given period of time (season, year) they coincide with the regenerated and new production

$$\Sigma L_d(1 - f_d) = R = P(1 - f),$$

$$\Sigma L_d f_d = X = Pf.$$

On the right-hand side of these equations, f is the bulk value supposed to be typical (and known) for the zone under consideration and used as a constraint, while the daily values f_d in the left-hand side are not necessarily constant. The capability of the model to account for such varying f_d is only used if information are available or if plausible hypothesis can be made about its variation. A reasonable hypothesis, for instance, consists in increasing f_d during the bloom period and tailoring its evolution according to the Chl biomass itself (see below).

The levels where the above processes occur must also be considered. When $Z_p > Z_{ml}$, the CO_2 regeneration happens within the mixed layer and below it. By approximation, R_d can be split into two terms, according to a mixing rule. The first term, $R_{d,ml}$, equally distributed inside the mixed layer, is expressed as

$$R_{d,ml} = R_d(Z_{ml}/Z_p)$$

and the second term, inside the stratified layer, is made depth-dependent according to

$$R_d(z) = R_d(1 - (Z_{ml}/Z_p))(P(z)/P_{tot})$$

where $P(z)$ and P_{tot} are the local and the column-integrated productions below the mixed layer, respectively. The approximate character of the above formulation comes from that the f_d values are considered as independent from depth, in spite of the possible difference between the two trophic or taxonomic status above and under the eddy diffusivity minimum. Oxygen and nitrate evolutions can be retrieved from the P and R values by using Redfield ratios (see Appendix F).

3.6. Practical application

An illustration of the above method is provided by simulating an annual cycle for a situation already studied by Taylor et al. (1991), hereafter denoted by TL. Their annual cycles of sea-surface Chl and mixed-layer depth, assumed to be typical of a station located at 35° N in the Atlantic ocean, are adopted. At this location, the biomass evolution is characterised by a phytoplankton bloom occurring in spring, when the mixed layer begins to be stabilised (Fig. 3). Net primary production is separately computed within and under the mixed layer, leading to a column-integrated production, P, of 84 gC m^{-2} y^{-1}. By summing the columns 1,

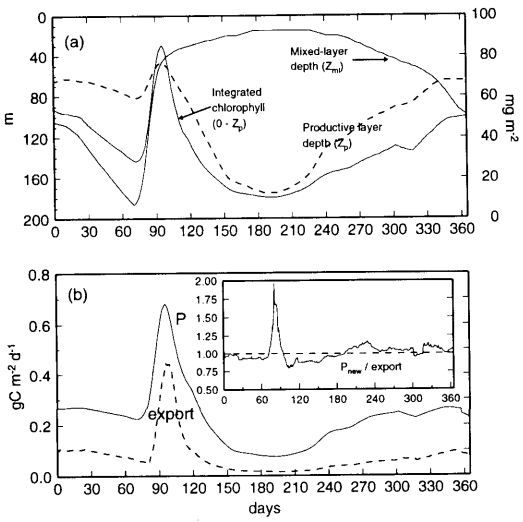

Fig. 3. Illustration of the method proposed to estimate the local recycling of organic carbon within the productive layer, and the export of organic matter toward deeper levels. An academic station is selected (see text, and panel (a)), characterized by a mixed-layer annual course, and an imposed Chl content which determine the depth of the productive layer in the present model. (b) Export from the productive layer is then estimated from P (see text for its calculation) combined with the temporal variations of the integrated Chl content. The annual course of the ratio of new production to export of organic carbon is shown in insert.

2 and 4 of the Table 2 in TL (sinking, diffusion of cells, and mortality), a value of 82 gC m^{-2} y^{-1} is obtained, comparable to the present primary production estimate. These results are obtained from the same sea-surface Chl cycle, the resulting integrated Chl contents being however quite different, as a consequence of different depths of integration; the depth considered in TL covers the mixed layer plus thermocline domain throughout the year, this domain being deeper or shallower than the depth of the productive layer (Z_p) taken into account in the present model. To estimate the net effect of biota on the ΣCO_2, the annual course of the f-ratio is assumed to mimic that of Chl, with a maximum coinciding with the spring bloom (arbitrarily set to 0.7), and a minimum occurring in summer (set to 0.2), leading to a mean value of 0.3 (a value generally believed to be typical of the open ocean; see, e.g., Platt et al., 1989). Under these assumptions, export from the Z_p domain is estimated to be 26 gC m^{-2} y^{-1}, firstly increasing like P when the bloom begins, and then rapidly decreasing to become nearly zero in summer, as recycling increases. New production (Pf) and export (Lf) exhibit different annual courses, whereas their values are equal when summed over the year. These features are to be compared with net, new and recycled production annual cycles as they can be obtained, for example, from detailed ecological models (see, e.g., Figs. 8 and 9 in Fasham et al., 1990), and leads to place some confidence in the presently proposed method for the estimation of the carbon export from the productive layer.

4. Conclusion

It was intended in the present work to develop a one-dimensional model, able to simulate the pCO_2 evolution within the oceanic mixed layer, in response to the physical forcing and biological activity. A second aim was to prepare numerical tools for the future use of a limited suite of parameters, measurable from remote-sensing platforms, to predict at global scale the CO_2 exchange at the air-sea interface. This second goal has entailed several constraints when developing the model, so that it differs from other, more classical approaches. A priori knowledge of the oceanic zone under consideration and a restricted set of climatological values are inevitably needed to start any computation of this kind. Beside this initial information, the input parameters for the model are deliberately limited to those detectable from space (Table 2). The main consequences of this choice can be summarised as follows.

There is no algal growth modelling in spite of the incrustation in the model of a sub-unit dealing with the photosynthetic activity. This segment actually is fed by the chlorophyll concentration, as observed within the upper layer, and it computes a daily carbon fixation. It is unable, per se, to predict the algal population evolution, as sinking, mortality, grazing rate and other ecological features are not parameterised.

The algal compartment is exclusively seen as a peculiar carbon compartment and not, as usual, as a nitrogen compartment. The dependence of phytoplankton growth on the nutrient(s) availability is not taken into account as such; it is implicitely involved in so far as the biomass

abundance (the Chl concentration) necessarily results from the past nutrient availability, for given radiative conditions. Therefore nitrate is not an input parameter in the model. Nitrate, like oxygen, can conversely be derived as a by-product of the simulation, via the Redfield's ratios.

The biological activity, summed up as a chemical, partly reversible, process, is simply represented by two antagonist functions, the net photosynthetic inorganic carbon uptake and the organic carbon loss (itself comprising two terms, the local regeneration and the export). The regulation of the system, and therefore the way of tuning the opposite effects of the two functions within the model, is based on the adoption of a mean f-value (new-to-total production ratio), and, if available, on information concerning the f-evolution along the seasons.

The present model has been validated and its sensitivity to parameter values has also been tested (Antoine and Morel, this issue) to gain a better understanding of the intricated dependences of the ΣCO_2 on the physical and biological processes.

5. Acknowledgements

We acknowledge support through the European community contracts EPOC-CT90-0017 and ESCOBA EV5V-CT92-0124. The authors would like to express their appreciation to Annick Bricaud, Jean-François Minster, Jean-Michel André, and one anonymous reviewer for valuable criticism and suggestions.

6. Appendix A. Sea-surface wind stress, and heat fluxes

The surface wind stress and heat fluxes fix the surface boundary conditions which drive the evolution of the eddy kinetic energy within the model of Gaspar et al. (1990). For the sake of completeness, the basic one-dimensional heat, salt and momentum equations forming the EKE model, and the corresponding surface conditions, are briefly recalled below (for further information about these equations and the kinetic energy closure scheme, the reader is referred to Gaspar et al., 1990)

$$\frac{\partial \bar{T}}{\partial t} = \frac{SW}{\rho_0 c_p}\frac{\partial E(z)}{\partial z} - \frac{\partial \overline{T'w'}}{\partial z}$$

with the surface condition

$$-\rho_0 c_p \overline{T'w'}(0) = F_{nsol} = Q_e + Q_c + LW,$$

$$\frac{\partial \bar{S}}{\partial t} = -\frac{\partial \overline{S'w'}}{\partial z}$$

with the surface condition

$$-\rho_0 c_p \overline{S'w'}(0) = E_V - P_R,$$

$$\frac{\partial \bar{U}}{\partial t} = -f\boldsymbol{k} \times \bar{U} - \frac{\partial \overline{U'w'}}{\partial z}$$

with the surface condition

$$-\rho_0 \overline{U'w'}(0) = \tau$$

T, S, U, and w are the temperature, salinity, horizontal and vertical velocities of the water, f is the Coriolis parameter, $\boldsymbol{k}$ the vertical unit vector, and τ is the surface wind stress; ρ_0 and c_p are the reference density and the specific heat of sea water, respectively; $E(z)$ is the fraction of the surface solar radiation which reaches the depth z. Q_e and Q_s are the latent and sensible heat fluxes, SW is the incoming solar radiation, LW is the net long-wave radiation budget, and $E_V - P_R$ is the water balance at the air-sea interface. These various terms are explicited below.

6.1. *Wind stress* τ

When not measured at 10 m height, the wind speed is transformed into its value at this elevation, V_{10} (m s^{-1}), by using the method of Kondo (1975), assuming a logarithmic wind profile. The dimensionless wind stress coefficient, C_{10}, is then computed according to Wu (1982):

$$10^3 C_{10} = 0.8 + 0.065 V_{10},$$

$$\text{and the wind stress} \quad \tau = \frac{\rho}{\rho_0} C_{10} V_{10}^2,$$

where ρ is the density of air (1.29 kg m^{-3}), and ρ_0 the reference density of sea water (1024.5 kg m^{-3}).

6.2. *Heat budget*

The heat budget at the sea surface is the sum of four terms, namely Q_e, the latent heat flux, Q_s, the sensible heat flux, SW, the incoming total solar radiation, and LW, the net long-wave radiation budget. These fluxes (all expressed as W m^{-2}) are estimated as follows:

6.3. Latent heat flux: Q_e

The latent heat flux, Q_e is estimated by using the bulk aerodynamic formula, as adapted by Friehe and Schmitt (1976):

$$Q_e = -C_D L_w V_{10}(q_s - q_a),$$

C_D is a drag coefficient ($=1.32 \cdot 10^{-3}$), L_w is the latent heat of sea water, namely $L_w = 10^3(2510 - 2.38\ \mathrm{SST})$ J kg^{-1}.

q_s, the absolute saturation humidity of air at the sea-surface temperature (SST), is $q_s = 100(P_S/R_V\ \mathrm{SST})$, expressed as kg m^{-3}, where P_S, the saturation pressure is, $P_S = 6.112 \exp(17.37\ \mathrm{SST}/(\mathrm{SST} + 238.8))$ (Buck, 1981), and $R_V = 461.5$ J kg^{-1} °K^{-1}.

q_a, the absolute humidity of the air (T_a is the air temperature) is: $q_a = 100(P_S/R_V T_a)$, expressed as kg m^{-3}, where P_S, the saturation pressure is computed from the dew point temperature, T_{dew}, $P_S = 6.112 \exp(17.37 T_{dew}/(T_{dew} + 238.8))$ if T_{dew} is greater than 0°C, $P_S = 6.112 \exp(22.54 T_{dew}/(T_{dew} + 273.48))$ if T_{dew} is lower than 0°C.

6.4. Sensible heat flux: Q_s

The sensible heat flux, Q_s is estimated by using the bulk aerodynamic formula, as adapted by Friehe and Schmitt (1976):

$$Q_s = -\rho c_p (A + C_h V_{10}(\mathrm{SST} - T_a)),$$

where c_p is the specific heat of air (1005 J kg^{-1} °K^{-1}) and A and C_h are regression coefficients (they replace, with the same meaning, the bulk transfer coefficient for sensible heat, usually noted C_H); A and C_h depend upon the product $X = V_{10}(\mathrm{SST} - T_a)$, depicting the stability of the air column:

if $0 \Leftarrow X \Leftarrow 25$

$A = 2 \cdot 10^{-3}$ and $C_h = 0.97 \cdot 10^{-3}$

if $X > 25$

$A = 0$ and $C_h = 1.46 \cdot 10^{-3}$

if $X < 0$

$A = 2 \cdot 10^{-3}$ and $C_h = 0.86 \cdot 10^{-3}$

6.5. Incoming total solar radiation: SW

The total downwelling solar radiation (wavelengths from 0.3 to 2.5 μm) incident at the sea surface under a clear sky (SW_{clear}), is computed by using the "5S" atmospheric radiative transfer model of Tanré et al. (1979, 1990), operated for standard atmospheric conditions, namely for a visibility of 23 km, an integrated ozone content of 350 DU and 2 cm of precipitable water. A departure from these mean conditions does not produce drastic changes in the estimate of total radiation. The "5S" model is operated once and for all to produce tabulated values for each wavelength between 0.3 and 2.5 μm (step 0.02 μm) and for 19 sun-zenith angles from 0 to 90 degrees. The actual value of solar radiation for given geographical locations and dates is then obtained by interpolating in the look up table.

Reduction of solar energy due to cloudiness is estimated according to Reed (1977):

$$SW = SW_{clear}\, C_r,$$

$$C_r = 1 - 0.632c + 0.0019\alpha.$$

SW is the radiation under cloudy conditions, where c, the cloud cover, is $N/8$, if N is the cloudiness expressed in okta (c ranges from 0 for a clear sky to 1 for overcast conditions) and α is the noon solar elevation in degrees. This formula is valid for cloud cover from 0.28 to 1.0. For low cloudiness ($c < 0.28$), C_r is given a constant value (0.95), as suggested by Reed (1977).

To account for the less severe absorption of the visible radiations (400–700 nm, i.e., the PAR domain), compared to that affecting the near IR domain (>700 nm), the C_r factor above is split into two distinct factors, $C_{r,vis}$ and $C_{r,ir}$, computed according to (Baker and Frouin, 1987; Morel and André, 1991):

$$C_{r,ir} = 0.75 C_{r,vis},$$

and by demanding that

$$SW = (SW_{clear,vis} + SW_{clear,ir})\, C_r$$
$$= SW_{clear,vis}\, C_{r,vis} + SW_{clear,ir}\, C_{r,ir}.$$

In this way, the cloud-induced reduction in the visible domain is only 75% of that in the near IR, whereas the reduction of the whole spectrum of solar radiations satisfies the Reed's formulation. Specular reflection at the air-sea interface is accounted for. Wind-dependent reflection coefficients for the direct radiation (Austin, 1974), are

used to compute the radiation just below the sea surface. Values for UV + visible and infrared radiations (from 300 to 2500 nm) are separately integrated to operate the solar heating parameterisation (Morel and Antoine, 1994). The spectral values in the visible domain (from 400 to 700 nm, with an increment of 20 nm) are computed to feed the spectral light-photosynthesis model (Appendices C and D).

6.6. The net long-wave radiation budget: LW

LW, which is the sum of the thermal radiation lost by the sea surface, and of the gain due to absorption of thermal radiation from the atmosphere, is computed by the Brunt's formula, as in Hastenrath and Lamb (1978), namely:

$$LW = [\varepsilon\sigma\ SST^4(0.39 - 0.056\sqrt{e})(1 - 0.53c^2)] + [4\varepsilon\sigma\ SST^3(SST - T_a)].$$

c is the cloudiness index, as above.

ε is the emissivity of the ocean (0.97)

σ is the Stefan-Boltzman constant ($5.67 \cdot 10^{-8}$ $Wm^{-2}\,°K^{-4}$)

e, the water vapor pressure, is $(r/(0.62197 + r))P_{atm}$ (Gill, 1982), where $r = q_a/(1 - q_a)$ and P_{atm} is the barometric pressure.

6.7. Water budget $E_V - P_R$

When an unbalance in the water budget occurs, salinity is changing according to the difference between the evaporation (see 6.3) and precipitation rates.

7. Appendix B. Inferring the *Chl* vertical profile from the $Chl_{\langle sat\rangle}$ value

The reconstruction of the Chl profiles from the concentration within the upper layer, $Chl_{\langle sat\rangle}$ (mg Chl m^{-3}), rests on the following equations (see in Morel and Berthon, 1989, for more details). The first step consists of relating $Chl_{\langle tot\rangle}$ (mg Chl m^{-2}), the integrated amount of Chl within the euphotic layer (depth Z_e) to $Chl_{\langle sat\rangle}$ according to

$$Chl_{\langle tot\rangle} = 37.9\ Chl_{\langle sat\rangle}^{0.548}$$

(for deep mixed layers)

$$Chl_{\langle tot\rangle} = 38\ Chl_{\langle sat\rangle}^{0.423}$$

(stratified waters, with $Chl_{\langle sat\rangle} < 1$ mg Chl m^{-3})

$$Chl_{\langle tot\rangle} = 40.3\ Chl_{\langle sat\rangle}^{0.505}$$

(stratified waters, with $Chl_{\langle sat\rangle} > 1$ mg Chl m^{-3})

The depth of the euphotic zone, Z_e, is derived from the pigment profile by using the optical model (Morel, 1988). For computational convenience two successive simple expressions can be used which directly relate Z_e to $Chl_{\langle sat\rangle}$ according to

$$Z_e = 568.2\ Chl_{\langle tot\rangle}^{-0.746}$$

(if $Z_e < 102$ m),

$$Z_e = 200\ Chl_{\langle tot\rangle}^{-0.293}$$

(if $Z_e > 102$ m).

The vertical profiles are computed in a dimensionless way by using the optical depth $\zeta = Z/Z_e$, and the relative concentration $X = Chl(\zeta)/\overline{Chl_{ze}}$, where $\overline{Chl_{ze}}$ is the mean concentration within the euphotic layer; the Gaussian profile is expressed as

$$Chl(\zeta)/\overline{Chl_{ze}} = Chl_{bg} + Chl_{max} \times \exp[-((\zeta - \zeta_{max})/\Delta\zeta)^2],$$

with the following meaning.

Chl_{bg} is a background concentration over which is superimposed the Gaussian peak. Chl_{max} represents the intensity of the deep Chl maximum, located at an optical depth ζ_{max} and with a vertical extension determined by $\Delta\zeta$. All these quantities (Chl_{bg}, Chl_{max}, ζ_{max} and $\Delta\zeta$) are related to $Chl_{\langle sat\rangle}$ (polynomials in eq. (6) of Morel and Berthon). The profiles actually extend beyond Z_e and the above equation produces values down to Z_p ($= 1.5Z_e$) as required for the present study. Reverting ζ and X into physical quantities (depth in meters and Chl in mg m^{-3}) is straightforward.

8. Appendix C. Propagation of the downwelling PAR within the water column and calculation of the primary production

The propagation within the water column of the PAR incoming at the sea level (see Appendix A for

its calculation) is computed by using a spectral model (Morel, 1988). This parameterisation differs from that used when assessing the solar heating, as spectrally detailed values for irradiance are needed in conjunction with the spectral values of algal absorption. For any wavelength, and at any depth z within the euphotic zone:

$$\mathrm{PAR}(z, \lambda) = \mathrm{PAR}(z - \mathrm{d}z, \lambda)\, \mathrm{e}^{(-K_\mathrm{d}(\lambda)\,\mathrm{d}z)}$$

where $K_\mathrm{d}(\lambda)$, the spectral diffuse attenuation coefficient for downwelling irradiance, is parameterised as:

$$K_\mathrm{d}(\lambda) = K_\mathrm{w}(\lambda) + \chi(\lambda)\,\mathrm{Chl}^{e(\lambda)},$$

where $K_\mathrm{w}(\lambda)$ is the attenuation coefficient for pure sea-water, and the $\chi(\lambda)$ factor and exponent $e(\lambda)$ were derived from regression analysis on log-transformed K_d spectra.

The integration with respect to wavelength is operated with a reduced number of wavelengths, from 61 in the initial version (Morel, 1991) to 16 for the present study; the wavebands are thus 20 nm wide instead of 5 nm. The consistency of primary production computed by using these two spectral resolutions has been checked, and there is no significant difference (see also Platt and Sathyendranath, 1991). Integration vis-a-vis time is operated over ten equal intervals within the daylength. With respect to depth, the computation of primary production is made with a depth increment of 5 m throughout the entire productive layer.

The production model is not operated differently when dealing with the mixed layer. The vertical pigment profile is assumed to be strictly uniform in the present modeling, so that the random motions of algal cells within the mixed layer must exactly compensate. To the extent that the primary production is computed by using a set of fixed physiological parameters, the misadaptation (if any) of algae to the varying light levels, experienced during the vertical motions, is not taken into account. With a constant chlorophyll concentration and a constant physiology, the production within a turbulent mixed layer is necessarily equal to that of a "frozen" layer.

The use of a "mean irradiance" within a mixed layer, $\overline{\mathrm{PAR}}_\mathrm{ml}$, has been recurrently proposed. This mean is obtained as

$$\overline{\mathrm{PAR}}_\mathrm{ml}/\mathrm{PAR}(0^-) = (Z_\mathrm{ml})^{-1} \int_0^{Z_\mathrm{ml}} \exp(-Kz)\,\mathrm{d}z$$

$$= (KZ_\mathrm{ml})^{-1}\,[1 - \exp(-KZ_\mathrm{ml})],$$

where $\mathrm{PAR}(0^-)$ is the irradiance just beneath the surface and K is the diffuse attenuation coefficient for downwelling PAR irradiance ("averaged" for the spectral range involved). This approximation is not acceptable because it ignores the non-linear character of the photosynthesis-irradiance response of algae (the so-called P versus E curve). An average value of this function which would result from the convolution of the P versus E curve with the depth-irradiance exponential decay would be a better approximation. It is easy to demonstrate that such an approximation is exactly that of the frozen layer, apart from the fact that the spectral aspect is discarded.

9. Appendix D. Summarized description of the spectral light-photosynthesis model

The spectral light-photosynthesis model of Morel (1991) is based on the integration of the growth rate equation of Kiefer and Mitchell (1983), and P, the daily carbon fixation within the productive column ($\mathrm{gC\,m^{-2}\,d^{-1}}$) is computed according to

$$P = 12 a^*_\mathrm{max} \varphi_{\mu,\mathrm{max}} \int_0^L \int_0^{Z_\mathrm{p}} \int_{400}^{700} \mathrm{Chl}(z)\,\mathrm{PUR}(\lambda, z, t)$$

$$\times f[x(z, t)]\,\mathrm{d}\lambda\,\mathrm{d}z\,\mathrm{d}t.$$

L is the daylength, Z_p the depth of the productive layer and 400–700 nm represents the spectral domain of photosynthetically active radiation (PAR). The meaning of the various terms is as follows: $\mathrm{Chl}(Z)$ describes the vertical Chl profile. The Chl-specific absorption spectrum of algae, denoted $a^*(\lambda)$, is transformed into

$$a^*(\lambda) = a^*_\mathrm{max} A^*(\lambda),$$

where a^*_max is the maximum value found in the $a^*(\lambda)$ spectrum (generally at 440 nm) and $A^*(\lambda)$ represents the (dimensionless) probability of absorption. $\mathrm{PUR}(\lambda, Z, t)$ is the photosynthetically usable radiation, i.e., the product $A^*(\lambda)$ $\mathrm{PAR}(\lambda, Z, t)$ where PAR is the scalar irradiance.

The quantum yield for growth, φ_μ, which depends on irradiance (actually on PUR) is expressed in a dimensionless way by forming the ratio

$$f(x) = \varphi_\mu / \varphi_{\mu,\max},$$

where x is a dimensionless descriptor of irradiance obtained as

$$x = \mathrm{PUR}/\mathrm{KPUR}$$

with

$$\mathrm{PUR} = \int_{400}^{700} \mathrm{PUR}(\lambda)\, \mathrm{d}\lambda$$

and KPUR is a scaling value.

The $f(x)$ function directly derives from the mathematical representation of the P^B versus E curve (production versus irradiance curve). The parameterization of Platt et al. (1980) is adopted, and leads to

$$f(x) = x^{-1}(1 - \mathrm{e}^{-x})\, \mathrm{e}^{-\beta x},$$

where β accounts for photoinhibition at high irradiance. The quantum yield is maximum at vanishing irradiance ($x \to 0, f(x) \to 1, \varphi_\mu \to \varphi_{\mu,\max}$) and decreases with increasing irradiance ($x \to \infty$, $f(x) \to 0$, $\varphi_\mu \to 0$). The scaling term KPUR fixes the irradiance level for which $f(x) = \frac{1}{2}$ (and $\varphi_\mu = \frac{1}{2}\varphi_{\mu,\max}$).

Knowing the spectral irradiance incident at the surface, $\mathrm{PAR}(\lambda, 0, t)$, its propagation through the water column is computed in relation to the $\mathrm{Chl}(Z)$ profile; $\mathrm{PUR}(\lambda, Z, t)$ is straightforwardly obtained as well as its spectrally integrated quantity which provides the local and instantaneous value of x and thus of $f(x)$. The integrations are performed with $\mathrm{d}\lambda = 20$ nm, $\mathrm{d}z = 5$ m, and $\mathrm{d}t = L/10$.

The quantities are given the following values:

$a^*_{\max} = 45\ \mathrm{m}^2\ (\mathrm{g\ Chl})^{-1}$;

$A^*(\lambda)$ is a mean spectrum for 14 species grown in culture (see in Morel, 1988);

$\varphi_{\mu,\max} = 0.07$ mol C (mol quanta)$^{-1}$;

KPUR $= 25.77\ \mu$mol quanta $\mathrm{m}^{-2}\,\mathrm{s}^{-1}$ at 20°C, and varies with temperature according to a van't Hoff dependency $\mathrm{KPUR}(\mathrm{T}^\circ) = \mathrm{KPUR}(20^\circ\mathrm{C})\ 1.065(\mathrm{T}^\circ - 20)$.

These values given to the physiological parameters are that adopted in Berthon and Morel (1992), and lead to a maximum production rate normalised to biomass ($P^B_{\max}$) equal to 3.31 gC g $\mathrm{Chl}^{-1}\,\mathrm{h}^{-1}$ at 20°C.

10. Appendix E. Carbonate chemistry

To initialise the model, ΣCO_2 and TA vertical profiles are needed, and are built as follows: within the entire mixed layer and for the deep reservoir, ΣCO_2 and TA are given values typical of the site under consideration (climatological values or measurements, if any), and are linearly interpolated between these two domains. A 2-year preliminary run of the model, fed with these vertical profiles, and making use of the forcing of the first year of simulation only, leads finally to the ΣCO_2 and TA vertical profiles thereafter used for initialisation. This procedure ensures coherence between the physical structure of the water column and the initial ΣCO_2 and TA vertical profiles.

From the actual values of temperature and salinity, the dissociation constants of carbonic acid K'_1 and K'_2 in mol kg^{-1} (and $K'_r = K'_1/K'_2$) are estimated following Goyet and Poisson (1989), the solubility of CO_2 in sea water (α, mol kg^{-1} atm^{-1}), following Weiss (1974). The borate concentration (BR), the dissociation constants for boric acid and sea water, respectively K_b and K_w, are calculated according to the international UNESCO equations (UNESCO, 1987). The following iterative procedure allows then the pCO_2 to be computed from ΣCO_2 and TA (the values for the hydrogen ion activity, H^+, and the carbonate alkalinity, CA, are also computed). Firstly, the variable A takes the value of TA, and the dissolved CO_2 concentration is estimated according to

$$[\mathrm{CO_2}] = \Sigma\mathrm{CO_2} - A + \left[\frac{AK'_r - \Sigma\mathrm{CO_2}K'_r - 4A + Z}{2(K'_r - 4)}\right],$$

where

$$Z = \sqrt{(\Sigma\mathrm{CO_2}K'_r)^2 + AK'_r(2\,\Sigma\mathrm{CO_2} - A)(4 - K'_r)},$$

$$H^+ = \frac{([\mathrm{CO_2}]\,K'_1)}{2A} + \frac{\sqrt{([\mathrm{CO_2}]\,K'_1)^2 + 8A[\mathrm{CO_2}]\,K'_1K'_2}}{2A}$$

$$CA = TA - BR\frac{K_b}{K_b + H^+} - \frac{K_w}{H^+} + H^+.$$

These three successive equations are repeated, the variable A taking now the successive values of CA, until the absolute value of the difference $(CA - A)$ becomes lower or equal to 10^{-8}. The iterations are then stopped, and the pCO_2 is estimated according to:

$$pCO_2 = \frac{\Sigma CO_2}{\alpha\left(1 + \frac{K'_1}{H^+} + \frac{K'_1 K'_2}{H^{+2}}\right)}.$$

For example, with a temperature of 15°C, a salinity of 37 psu, a ΣCO_2 of 2000 μmol kg^{-1} and a total alkalinity of 2250 μeq kg^{-1}, the computed pCO_2 is 350.017 μatm, carbonate alkalinity is 2112.05 μeq kg^{-1} and PH is 8.075. When this procedure is operated by using the inputs proposed by Peng et al. (1987) to test their own method, pCO_2 is found to be 777.04, whereas their estimate is 769.79 (bearing in mind that their calculations account for the weak influence of silicic and phosphoric acids on seawater total alkalinity, and that they use a different set of constants for the dissociation of carbonic acid).

It is worth noting that when pCO_2, ΣCO_2 and TA are simultaneously measured at sea, the pCO_2 that can be computed, from the measured values of ΣCO_2 and TA, and from appropriate dissociation constants, often exhibits a difference with the measured pCO_2 (up to 30 μatm), depending upon the set of constants used, and also upon the measurement protocol (see, e.g., UNESCO, 1987; Goyet et al., 1991). These discrepancies are not yet well explained, but they must be kept in mind when comparing pCO_2 from the model to measured pCO_2.

11. Appendix F. Detailed equations and numerical methods

The equation governing the daily variation of ΣCO_2, TA, O_2 and NO_3 at any depth within the water column is (thereafter, S stands either for ΣCO_2, TA, NO_3 or O_2)

$$\frac{\partial S}{\partial t} = J + \frac{\partial K_z}{\partial z}\frac{\partial S}{\partial z} + K_z\frac{\partial^2 S}{\partial z^2}. \quad (1)$$

K_z is the eddy diffusivity, and J is the net biologically-induced consumption (or release) of CO_2, TA, NO_3 or O_2.

$$J_{\Sigma CO_2} = -P + R,$$

$$J_{TA} = \left[-P\frac{C_{org} + C_{carb}}{C_{org}}\right]\left[\left(2\frac{C_{carb}}{C_{org} + C_{carb}}\right) - \left(N/C\frac{C_{org}}{C_{org} + C_{carb}}\right)\right],$$

$$J_{NO_3} = -PfN/C,$$

$$J_{O_2} = (PfO_2/C) + (P(1-f)) - R.$$

P, R and f have been previously defined in the text. N/C is the stoechiometric molar ratio (Redfield ratio) depicting the relative proportion under which nitrogen and carbon are assimilated by phytoplankton ($N/C = 15/106$), O_2/C is the Redfield ratio of oxygen to carbon (138/106). Ammonium is the nitrogen source for the recycled production ($P(1-f)$), and it is also the end-product of regeneration (R). Thus, in the last two terms of the equation for J_{O_2}, the ratio O_2/C is assumed to be unity (i.e., 106/106). Concerning J_{TA}, C_{carb} and C_{org} stand for carbon assimilated via the fixation of calcium carbonate, and via the formation of soft tissues. The typical ratio $4C_{org}$ for $1C_{carb}$ (Broecker and Peng, 1982) can be used. P only concerns the formation of soft tissues, so its value, in the equation for J_{TA}, is at first multiplied by the ratio of the total carbon assimilation to that realised via the formation of soft tissues. In the second bracket, the first term stands for the effect of calcium carbonate fixation, and the second one for the effect of nitrate uptake.

The mixed layer is treated as a boundary layer and the concentration S (subscript ml is for mixed layer, and z_0 for the layer just below it) is modified following:

$$Z_{ml}\frac{\Delta S_{ml}}{\Delta t} = J_{s,ml} + F + K_{z,ml}\frac{S_{z0} - S_{ml}}{\Delta z}. \quad (2)$$

Δz is 5 m, and Δt is one day. F is the net flux at the ocean-atmosphere interface. F is either $(k\alpha\,\Delta pCO_2)$, or $(k\beta\,\Delta pO_2)$, or zero, for CO_2, O_2 and NO_3 respectively. k is the gas-transfer velocity between atmosphere and surface waters (m d^{-1}), ΔpCO_2 and ΔpO_2 are the partial pressure differences between atmosphere and surface-ocean, α and

β are solubilities (mol m^{-3} μatm^{-1}), respectively for CO_2 (Weiss, 1974) and O_2 (Weiss, 1970). $K_{z,ml}$ is the eddy diffusivity at the base of the mixed layer. If salinity is changing, TA is also modified according to $TA_{t+\Delta t} = TA_t^* \rho_{psu}$, where ρ_{psu} is the ratio of the salinities at times $t+\Delta t$ and t. This formulation is valid under the assumption of a constant specific alkalinity.

At the end of a day, the effect of entrainment, if any, is estimated (the mixed-layer depth being now Z_{ml1})

$$S_{ml} = \left[Z_{ml} S_{ml} + \int_{Z_{ml}}^{Z_{ml1}} S_z \, dz \right] \Big/ Z_{ml1} \qquad (3)$$

Eqs. (1) and (2) are solved by using the Crank-Nicolson method: the concentrations for the mixed layer and for each depth below it at the $(n+1)$th time step are computed from their values at the nth step by means of the finite difference approximation. The system is solved by iterations, which are initialised with the value at the $(n+1)$th step equal to the value at the nth step. Entrainment (eq. (3)), if any, is operated at the end of these computations and the ionic balance is applied to estimate pCO_2 from ΣCO_2 and TA. By using $\Delta t = 1$ day, and $\Delta z = 5$ m (that is relatively large time and space resolutions), numerical instabilities are sometimes, albeit rarely, encountered. This shortcoming is solved by halving Δt until stability is reached (practically, only one halving is enough to attain stability). The scheme for the finite differences approximation is:

(i) for the mixed layer

$$\Delta S_{ml} = \left[J_{ml} + \frac{F}{Z_{ml}} + \frac{1}{Z_{ml}} K_{z,ml} \frac{S_{z0} - S_{ml}}{\Delta z} \right] \Delta t;$$

(ii) for the layer just below it (z_0), which is the boundary between the mixed layer and the water column

$$\Delta S_{z0} = \left[J_{z0} + \frac{1}{\Delta z} K_{z,ml} \frac{S_{ml} - S_{z0}}{Z_{ml}/2} + \frac{1}{\Delta z} K_{z,z0} \frac{S_{z0+\Delta z} - S_{z0}}{\Delta z} \right] \Delta t;$$

(iii) for any depth within the water column, from $z_0 + \Delta z$ to $z_{deep} - \Delta z$:

$$\Delta S_z = \left[J_z + \frac{(K_z(z+\Delta z) - K_z(z-\Delta z))}{2\,\Delta z} \times \frac{(S(z+\Delta z) - S(z-\Delta z))}{2\,\Delta z} + K_z \frac{S(z+\Delta z) + S(z-\Delta z) - 2S(z)}{\Delta z^2} \right] \Delta t;$$

(iv) and for the deep reservoir

$$\Delta S_{deep} = 0.$$

REFERENCES

Antoine, D. and Morel, A. 1995. Modelling the seasonal course of the upper-ocean pCO_2. 2-Validation of the model and sensitivity studies. *Tellus*, this issue.

Austin, R. W. 1974. The remote sensing of spectral radiance from below the ocean. In: *Optical aspects of oceanography* (eds. N. G. Jerlov and E. S. Nielsen). Academic, San Diego, California, 317–344.

Baker, K. S. and Frouin, R. 1987. Relation between photosynthetically available radiation and total insolation at the ocean surface under clear skies. *Limnol. Oceanogr.* **32**, 1370–1377.

Berthon, J. F. and Morel, A. 1992. Validation of a spectral light-photosynthesis model and of its use in conjunction with pigment observations from space. *Limnol. Oceanogr.* **37**, 781–796.

Broecker, W. S. and Peng, T. H. 1982. *Tracers in the sea.* Eldigeo Press, Lamont-Doherty Geological Observatory, Palisades, NY, 690 pp.

Buck, A. L. 1981. New equations for computing vapor pressure and enhancement factor. *J. Appl. Meteorol.* **20**, 1527–1532.

Dugdale, R. C. and Goering, J. J. 1967. Uptake of new and regenerated forms of nitrogen in primary productivity. *Limnol. Oceanogr.* **12**, 196–206.

Eppley, R. W. 1972. Temperature and phytoplankton growth in the sea. *Fish. Bull.* **70**, 1063–1085.

Eppley, R. W. and Peterson, B. J. 1979. Particulate organic matter flux and planktonic new production in the deep ocean. *Nature* **282**, 677–680.

Fasham, M. J. R., Ducklow, H. W. and Mckelvie, S. M. 1990. A nitrogen-based model of plankton dynamics in the oceanic mixed layer. *J. Mar. Res.* **48**, 591–639.

Friehe, C. A. and Schmitt, K. F. 1976. Parameterization of air-sea interface fluxes of sensible heat and moisture by the bulk aerodynamic formulas. *J. Phys. Oceanogr.* **6**, 801–809.

Garcon, C., Thomas, F., Wong, C. S. and Minster, J. F. 1992. Gaining insight into the seasonal variability of CO_2 at ocean station P using an upper ocean model. *Deep-Sea Res.* **39**, 921–938.

Gaspar, P., Gregoris, Y. and Lefevre, J. M. 1990. A simple eddy kinetic energy model for simulations of the oceanic vertical mixing: tests at station Papa and long-term upper ocean study site. *J. Geophys. Res.* **95**, 16179–16193.

Gill, A. E. 1982. *Atmosphere-ocean dynamics.* Academic Press, New York, International geophysics series 30, 663 pp.

Goldman, J. C. and Brewer, P. G. 1980. Effect of nitrogen source and growth rate on phytoplankton-mediated changes in alkalinity. *Limnol. Oceanogr.* **25**, 352–357.

Gordon, H. R. and McCluney, W. R. 1975. Estimation of the depth of sunlight penetration in the sea for remote sensing. *Appl. Opt.* **14**, 413–416.

Gordon, L. I., Park, P. K., Kelley, J. J. and Hood, D. W. 1973. Carbon dioxide partial pressures in North Pacific surface waters (2). General late summer distribution. *Mar. Chem.* **1**, 191–198.

Goyet, C. and Poisson, A. 1989. New determination of carbonic acid dissociation constants in sea water as a function of temperature and salinity. *Deep-Sea Res.* **36**, 1635–1654.

Goyet, C., Beauverger, C., Brunet, C. and Poisson, A. 1991. Distribution of carbon dioxide partial pressure in surface waters of the Southwest Indian ocean. *Tellus* **43B**, 1–11.

Hastenrath, S. and Lamb, P. J. 1978. *Heat budget atlas of the tropical Atlantic and eastern Pacific oceans.* The University of Wisconsin press. Madison, Wisconsin.

Jerlov, N. G. 1976. *Marine optics.* Elsevier Oceanographic series 14, Elsevier, 231 pp.

Kempe, S. and Pegler, K. 1991. Sinks and sources of CO_2 in coastal seas: the North sea. *Tellus* **43B**, 224–235.

Kondo, J. 1975. Air-sea bulk transfer coefficients in diabatic conditions. *Boundary-layer Meteorol.* **9**, 91–112.

Laws, E. A. 1991. Photosynthetic quotients, new production and net community production in the open ocean. *Deep-Sea Res.* **38**, 143–167.

Legendre, L. and Gosselin, M. 1989. New production and export of organic matter to the deep ocean: consequences of some recent discoveries. *Limnol. Oceanogr.* **34**, 1374–1380.

Lewis, M. R., Cullen, J. J. and Platt, T. 1983. Phytoplankton and thermal structure in the upper ocean: consequence of nonuniformity in chlorophyll profile. *J. Geophys. Res.* **88**, 2565–2570.

Liss, P. S. and Merlivat, L. 1986. Air-sea gas-exchange rates: introduction and synthesis. In: *the role of air sea gas exchange in geochemical cycling* (ed. P. Buat-Menard). NATO ASI series 185, 113–128.

Longhurst, A. R. 1991. Role of the marine biosphere in the global carbon cycle. *Limnol. Oceanogr.* **36**, 1507–1526.

Metzl, N., Beauverger, C., Brunet, C., Goyet, C. and Poisson, A. 1991. Surface water carbon dioxide in the Southwest Indian sector of the Southern ocean: a highly variable CO_2 source/sink region in summer. *Mar. Chem.* **35**, 85–95.

Morel, A. 1988. Optical modelling of the upper ocean in relation to its biogenous matter content (case 1 waters). *J. Geophys. Res.* **93**, 10749–10768.

Morel, A. 1991. Light and marine photosynthesis: a spectral model with geochemical and climatological implications. *Prog. Oceanogr.* **26**, 263–306.

Morel, A. and André, J. M. 1991. Pigment distribution and primary production in the Western Mediterranean as derived and modelled from space (CZCS) observations. *J. Geophys. Res.* **96**, 12685–12698.

Morel, A. and Antoine, D. 1994. Heating rate within the upper ocean in relation to its bio-optical state. *J. Phys. Oceanogr.* **24**, 1652–1665.

Morel, A. and Berthon, J. F. 1989. Surface pigments, algal biomass profiles, and potential production of the euphotic layer: relationships reinvestigated in view of remote-sensing applications. *Limnol. Oceanogr.* **34**, 1545–1562.

Paulson, C. A. and Simpson, J. J. 1977. Iradiance measurements in the upper ocean. *J. Phys. Oceanogr.* **7**, 952–956.

Peng, T. H., Takahashi, T., Broecker, W. S. and Olafsson, J. 1987. Seasonal variability of carbon dioxide, nutrients and oxygen in the Northern North Atlantic surface water: observations and a model. *Tellus* **39B**, 439–458.

Platt, T., Gallegos, C. L. and Harrison, W. G. 1980. Photoinhibition of photosynthesis in natural assemblages of marine phytoplankton. *J. Mar. Res.* **38**, 687–701.

Platt, T. and Sathyendranath, S. 1988. Oceanic primary production: estimation by remote sensing at local and regional scales. *Science* **241**, 1613–1620.

Platt, T., Harisson, W. G., Lewis, M. R., Li, W. K. W., Sathyendranath, S., Smith, R. E. and Vezina, A. F. 1989. Biological production of the oceans: the case for a consensus. *Mar. Ecol. Prog. Ser.* **52**, 77–88.

Platt, T. and Sathyendranath, S. 1991. Biological production models as elements of coupled, atmosphere-ocean models for climate research. *J. Geophys. Res.* **96**, 2585–2592.

Quiñones, R. A. and Platt, T. 1991. The relationship between the *f*-ratio and the P:R ratio in the pelagic ecosystem. *Limnol. Oceanogr.* **36**, 211–213.

Reed, R. K. 1977. On estimating insolation over the ocean. *J. Phys. Oceanogr.* **7**, 482–485.

Robertson, J. E. and Watson, A. J. 1992. Thermal skin effect of the surface ocean and its implications for CO_2 uptake. *Nature* **358**, 738–740.

Schneider, B., Kremling, K. and Duinker, J. C. 1992. CO_2 partial pressure in Northeast Atlantic and adjacent shelf waters: processes and seasonal variability. *J. Mar. Sys.* **3**, 453–463.

Tanré, D., Herman, M., Deschamps, P. Y. and De Leffe, A. 1979. Atmospheric modelling for space

measurements of ground reflectances, including bidirectionnal properties. *Applied Optics* **18**, 3587–3594.

Tanré, D., Deroo, C., Duhaut, P., Herman, M., Morcrette, J. J., Perbos, J. and Deschamp, P. Y. 1990. Description of a computer code to simulate the satellite signal in the solar spectrum: the 5S code. *Int. J. Remote Sensing* **11**, 659–668.

Taylor, A. H., Watson, A. J., Ainsworth, M., Robertson, J. E. and Turner, D. R. 1991. A modelling investigation of the role of phytoplankton in the balance of carbon at the surface of the North Atlantic. *Global Biogeochem. Cycles* **5**, 151–171.

Thomas, F., Garçon, V. and Minster, J. F. 1990. Modeling the seasonal cycle of dissolved O_2 in the upper ocean at OWSP. *Deep-Sea Res.* **37**, 463–491.

Thomas, F., Minster, J. F., Gaspar, P. and Gregoris, Y. 1993. Comparing the behaviour of two ocean surface models in simulating dissolved O_2 concentration at OWSP. *Deep-Sea Res.* **40**, 395–408.

UNESCO 1987. Thermodynamics of the carbon dioxide system in seawater. Report by the carbon dioxide subpanel of the joint panel on oceanographic tables and standards. *Unesco Technical papers in Marine Science* **51**, 3–13.

Volk, T. and Liu, Z. 1988. Controls of CO_2 sources and sinks in the earth scale surface ocean: temperature and nutrients. *Global Biogeochem. Cycles* **2**, 73–89.

Volk, T. and Bacastow, R. 1989. The changing patterns of ΔpCO_2 between ocean and atmosphere. *Global Biogeochem. Cycles* **3**, 179–189.

Wanninkhof, R. 1992. Relationship between wind speed and gas exchange over the ocean. *J. Geophys. Res.* **97**, 7373–7382.

Watson, A. J., Robinson, C., Robinson, J. E., Williams, P. J. Le B. and Fasham, M. J. R. 1991. Spatial variability in the sink for atmospheric carbon dioxide in the North Atlantic, *Nature* **350**, 50–53.

Weiss, R. F. 1970. The solubility of nitrogen, oxygen and argon in water and seawater. *Deep-Sea Res.* **17**, 721–735.

Weiss, R. F. 1974. Carbon dioxide in water and seawater: the solubility of a non ideal gas. *Mar. Chem.* **2**, 203–215.

Weiss, R. F., Jahnke, R. A. and Keeling, C. D. 1982. Seasonal effects of temperature and salinity on the partial pressure of CO_2 in seawater. *Nature* **300**, 511–513.

Wong, C. S. and Chan, Y. H. 1991. Temporal variations in the partial pressure and flux of CO_2 at ocean station P in the subarctic northeast Pacific ocean. *Tellus* **43B**, 206–223.

Wong, C. S., Chan, I. Y., Page, J. S., Smith, G. E. and Bellegay, R. D. 1993. Changes in equatorial CO_2 flux and new production estimated from CO_2 and nutrient levels in Pacific surface waters during the 1986/87 El Niño. *Tellus* **45B**, 64–79.

Wu, J. 1982. Wind-stress coefficients over sea surface from breeze to hurricane. *J. Geophys. Res.* **87**, 9704–9706.